Journal of Advanced Research in Applied Sciences and Engineering Technology

Journal homepage:
https://semarakilmu.com.my/journals/index.php/applied_sciences_eng_tech/index
ISSN: 2462-1943

Evaluating the Binding Interactions between Artemisinin and Kelch 13 Protein Mutants Via Molecular Modelling and Docking Studies

Aisya Nazura Azman[1,2], Safwan Fathi Muhd Fahmirauf[1], Fazia Adyani Ahmad Fuad[1,*], Raden Shamilah Radin Hisam[2], Noor Azian Md. Yusuf[2]

[1,] Department of Chemical Engineering & Sustainability, Kulliyyah of Engineering, International Islamic University. Malaysia (IIUM), Jalan Gombak, 53100 Kuala Lumpur, Malaysia
[2] Parasitology Unit, Infectious Disease Research Centre, Institute for Medical Research, National Institute of Health, Setia Alam, Malaysia

ARTICLE INFO

Article history:
Received 13 September 2022
Received in revised form 2 Nov. 2022
Accepted 3 November 2022
Available online 30 November 2022

Keywords:
Malaria, *Plasmodium falciparum* parasites, artemisinin

ABSTRACT

Malaria is a parasitic infection caused by protozoan parasites from the genus *Plasmodium*. Over the years, various concerns have arisen regarding the efficacy in treating malaria caused by *Plasmodium falciparum*, which was reported to be caused by mutations in one of the parasite's proteins, known as the Kelch 13 (K13). This study aims to generate the model structures of *P.falciparum* K13 protein mutants and to evaluate the binding affinities and interactions between these proteins and artemisinin drug, which is the drug used for the treatment of malaria. To date, the interactions between the protein mutants and artemisinin drug have not been computationally elucidated. In this study, four different types of mutant proteins were analysed, which are V494I, L598G, S600C and N537I and the results were compared with the wild-type K13 protein. Homology models of these proteins were created using the wild-type K13 (PDB ID:4YY8), with high percentage of sequence identity with the mutants. Most models with -2 and 2 have good Rama-Z scores, hence it can be deduced that the four mutants V494I (-1.21 ± 0.42), L598G (-1.19 ± 0.41), S600C (-0.93 ± 0.43), N537I (-1.16 ± 0.43) and the wild-type (-1.34 ± 0.45) have acceptable Rama-Z scores. Molecular docking between artemisinin and the generated models of K13 proteins revealed that all protein mutants have higher binding energy; V494I (-6.79 kcal/mol), L598G (-9.26 kcal/mol), S600C (-6.17 kcal/mol) and N537I (-6.96 kcal/mol), compared to the wild-type (-9.65 kcal/mol). The results showed that all four distinct mutant proteins have less stable complex formation, which indicate that the mutant proteins have higher resistance towards artemisinin due to the higher binding energy compared to the K13 wild-type protein. However, all mutations have a higher number of protein-ligand hydrophobic interactions and protein-ligand hydrogen bonds than the wild-type protein, which requires further analysis to understand the binding interactions. The predicted structural information with regards to binding interactions between the K13 mutant proteins and artemisinin obtained from this study has paved the path toward understanding how mutants may cause parasites' resistance towards artemisinin drugs.

* *Corresponding author.*
E-mail address: fazia_adyani@iium.edu.my

https://doi.org/10.37934/araset.28.3.272286

1. Introduction

Plasmodium vivax, P.falciparum, P.ovale, and P.malariae are the four protozoan parasite species that cause malaria and are spread by the vector *Anopheles* mosquitoes [1]. In 85 countries where the disease is endemic, 227 million cases of malaria were reported back in 2019 and an increase was observed, where 241 million cases were reported in 2020. Artemisinin combination therapy (ACT) based on artemisinin (ART) is the first-line global treatment method for malaria. These compounds are activated in the parasite by Fe^{2+}-heme, which is made from hemoglobin [2,3]. The resistance of *P. falciparum* towards ART therapy has spread throughout the Greater Mekong Subregion (GMS) since it first appeared in Western Cambodia. Resistance is defined as a parasite clearance half-life of more than 5.5 hours [4]. Resistance to the first-line combination treatment piperaquine threatens efforts to control malaria in the GMS, where ART-resistant parasites have recently appeared and spread. Even though Malaysia has not yet reported any ART resistance cases, the ACT was shown to take a longer time to clear the parasites. Based on the reports from the Institute for Medical Research (IMR), the frequency of the *P. falciparum* Kelch 13 (*Pf*K13) polymorphisms were found to be candidates or linked to resistance in two samples from the East Coast of Peninsular Malaysia and one sample from the South Coast of Peninsular Malaysia.

One of the crucial *P.falciparum* proteins, K13, contains the BTB (Broad-complex, tramtrack and bric-à-brac) and Kelch-repeat propeller (KREP) domains. It was reported that *P. falciparum* is resistant to ART because it has mutations in the K13 (*Pf*K13) protein. *Pf*K13 plays a key part in the growth and division of asexual red blood cells, although the purpose of this protein is still unclear. It typically presents in E3 ubiquitin ligase complexes that aim to degrade a protein substrate by ubiquitin [5]. However, improper function of the K13 propeller causes permanent activation of transcriptional changes that "prime" the *Plasmodium* to resist oxidative drug damage [6]. Hence, studies on the function and mechanism of the K13 protein in the parasites, especially in *P.falciparum* is very much needed [7].

In this study, the interactions between the wild-type K13 and the mutants with ART were elucidated *via* a computational approach, in order to understand the effect of gene mutation on the effectiveness of antimalarial drugs. In order to study the binding interactions, comparative modelling of the mutant proteins was performed to generate an atomic-resolution model of a "target" protein from its amino acid sequence and the experimental three-dimensional structure of a related homologous protein. The strength of the interactions between two or more molecules, which are ART and mutated K13 proteins, were analyzed to predict how strong the drug binds to the target protein. In this case, hydrophobic interactions and hydrogen bonds indicate the presence of binding activities between the receptor and the ligand. Meanwhile, lower negative values of binding energy indicate a less stable complex that affects the functions of the compound [8]. These analyses might show the effects of mutation on ART efficacy.

The first step which is crucial in developing the most popular biological models, such as phylogenetic reconstruction, structural homology modelling, and functional inference through domain profile comparisons is multiple sequence alignment (MSA) [9]. T-Coffee builds libraries based on externally generated alignments rather than explicitly aligning sequences. It creates a coloured alignment in (.html) and (.pdf) format, with each residue appearing on a background displaying the alignment's quality. The T-Coffee package includes an implementation of the transitive consistency score (TCS) evaluation and filtering mechanism. The TCS server, a web-based application, determines the most precise regions in any pre-computed multiple sequence alignment, irrespective of the aligner. The TCS server allows deviation from similarity-based filtering techniques, such as Gblocks

and trimAl, while maintaining additional tree-estimation data. This server minimises misalignment in biological analyses. The RNA alignment capacity of TCS will be increased [10].

Meanwhile, molecular docking permits the investigation of any protein interactions, including protein-ligand interactions, as demonstrated by the case study of *P. falciparum* protein mutants towards the ART drug. This was performed to determine how tightly a ligand (ART) binds to a certain area of a protein, specifically the receptor-binding domain, also known as a coiled-coil-containing domain (CCC) in amino acid sequences between 212 and 314. These were the most conserved and contained the vast majority of K13 alleles related to ART [5]. To date, the effect of point-mutations in K13 protein on ART drug has not yet been established and no study has been attempted computationally to understand the interactions of this protein and the drug, which could be promising in combating ART drug resistance cases and eradicating malaria disease [11].

2. Materials and Methods

2.1. Sequence Alignment

The four protein mutants (V494I, L598G, S600C and N537I) sequences were obtained from the sequencing results of Azian and colleagues at IMR, Malaysia [12]. These sequences were used to find the matches in databases to obtain the template sequence. Subsequently, the template and the protein mutants' sequences were aligned to create MSA. The T-coffee was used to import the MSA in fast alignment (FASTA) format. By analysing the aligned sequences, the website determined the TCS. By default, the server computes a Mproba pair T-Coffee pairwise library and generates filtered alignments in addition to its other outputs, eliminating those columns with a scaled ColumnTCS score (range 0–9) below 4.

2.2. Modelling K13 Protein

BLAST was used to identify which protein to be utilised to create the model based on the DNA sequences that have been converted into RNA sequences, using BioEdit software version 7.2. Based on BLAST results, there are two related proteins in the data bank. K13 protein from *P. falcipa*rum (PDB ID: 4YY8) and K13 protein from *P. falciparum* (with disulfide bond) (PDB ID: 4ZGC), in which both are identical. However, 4YY8 has the most similar BLAST findings, which indicate its suitability to be used as the template for modelling. To complete the model, additional atoms and loops were introduced and optimized during the following construction stage.

Sidechain modelling is essential for studying protein-ligand and protein-protein interactions at the active sites and contact surfaces. Most modelling methods include sidechain refinement. UNIX software SCWRL (sidechain placement with rotamer library) was fast, and it uses the backbone-dependent rotamer library to insert side chains.

The last stage includes refinement and optimization, where it was needed for modelling, in light of the energy-related elements that are considered. Unfavorable bond angles, bond lengths, and near-atomic interactions were removed from the raw homology model to improve the model's validity. The energy-reduction method helps fix model flaws as for structural refinement, a molecular dynamics simulation may employ GROMOS, a UNIX application. Using MolProbity's Ramachandran Plot, the model quality was determined, where the final homology model must obey physicochemical principles.

2.3 Molecular Docking

To construct the ligand preparation file, the Structure Data File (SDF) of ART was downloaded from the PubChem website and converted to the PDBQT (Protein Data Bank, Partial Charge (Q), & Atom Type (T)) format using the Open Babel software. Docking was then performed after all preparatory procedures had been finished, signifying that both protein and ligand libraries have been processed and prepared appropriately. The result is a set of files consisting of an SDF output file and docking posture and score files for each ligand. The following is the structure of the output, where the files will be analysed, the scores from the SDF files will be retrieved, and the best score received thus far for each file will be chosen. All necessary files consist of the protein file (the completed model protein mutant), the ligand file (ART) that were both in PDB format and the Autodock executable file. By setting the preference file to this prepared file, the protein file was then opened to facilitate computations and to free the binding pocket of possible water molecules that could otherwise disturb the pose search.

The protein file was then prepared for docking after the PDBQT ligand file was added *via* the software interface's ligand option. Using the available possibilities, the torsion tree was determined. All of the ART examined in this study exhibits three torsion angles between the atomic planes. Once the ligand was prepared for docking, the grid for docking (receptor) was supplied, precisely as it would be when calculating docking using Autodock Vina. Blind docking happens when the following grid size (i.e., grid box dimensions) entirely covers the protein contact area. By highlighting all of the residues in the binding site, the modification is made simpler, and they were saved in the Grid Parameter File (GPF) format before executing the AutoGrid.

The Docking Log File (DLG) format was set as the parameter file prior to executing Autodock. The genetic algorithm was modified based on the amount of torsion. Since the number of torsions in all proteins utilised in this work spans from 1 to 10, only 50 GA runs and a population of 300 were established. The result of the DLG file was then saved as a Lamarckian Genetic Algorithm (LGA) variation for flexible ligand-receptor docking that is capable of handling a large number of degrees of freedom. The hybrid technique for molecular complex local optimization merged a multi-deme LGA with a previously reported gradient-based method.

3. Results and Discussion

3.1 Sequence Alignment Score

To predict a higher quality model of the query protein by homology modelling, it is required to align the template sequences well with closely similar template models by using T-Coffee. Utilising up weight or filtering scoring positions to demonstrate the use of proper simulation and empirical benchmarks enables the construction of a significantly more accurate phylogenetic tree, and for the majority of alignment methods, TCS. After post-processing, the base, nearly identical precision is achieved. The MSA results are shown in Figure 1.

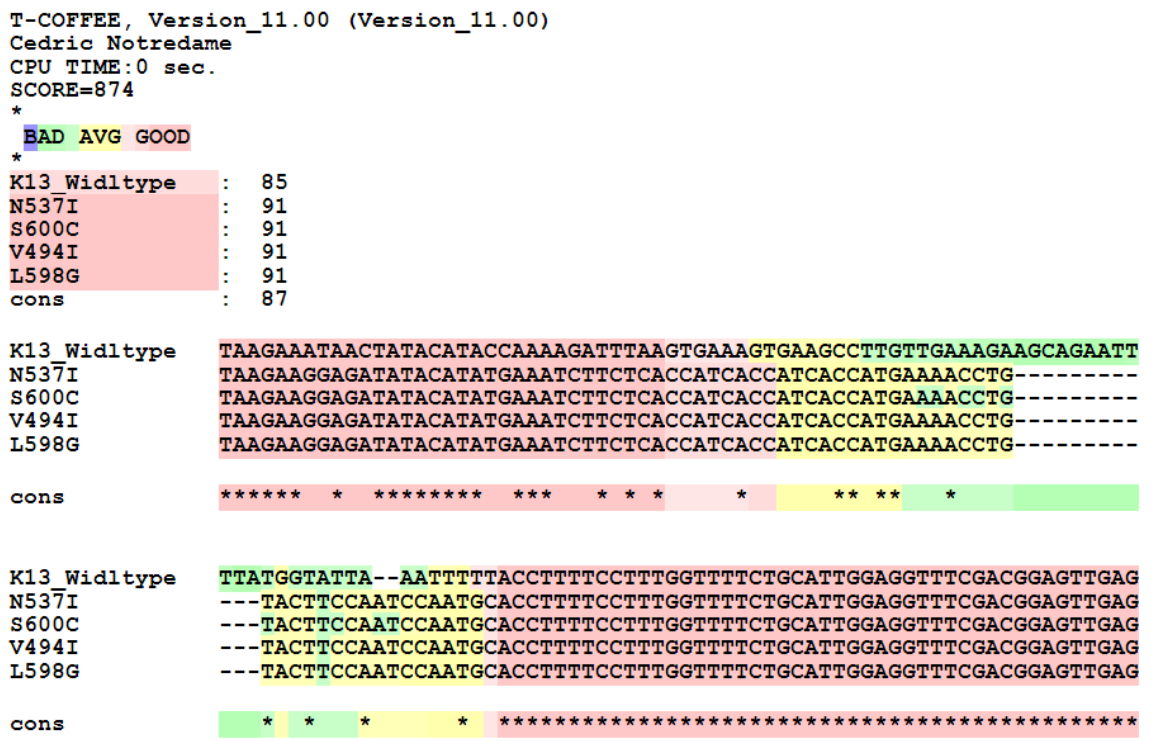

Fig. 1. The multiple sequence alignment retrieved from T-Coffee in HTML output format. Red indicates identical regions, whilst green and yellow indicate the less conserved regions

The red colour indicates that the regions in all sequences are identical. These regions are under high selection pressure and are critical for the proper function and structure of the DNA. Meanwhile, regions in green and yellow colour are less conserved regions. This alignment gives the ideas of the conservation of the protein mutants and the wild-type. Below the alignment is a line containing the consensus value (ColumnTCS) for each column. The K13 wild-type TCS score was found to be 85, while 91 for the mutations V494I, L598G, S600C, and N537I, and 87 for the final consensus (the nucleotide or amino acid residue that occurs most frequently at each site), respectively. Here, we demonstrate how our index, the TCS, may also be used to detect appropriately aligned residues as determined by structural analysis. The next stage of homology modelling was carried out using the generated templates.

3.2 Homology Modelling of Kelch 13 Protein Structures

One of the metrics for evaluating model quality that was added to MODELLER is Discrete Optimised Protein Energy (DOPE). DOPE is a statistical potential that depends on the atomic distance inferred from a sample of native protein structures [13,14]. The best protein model based on the discrete optimized protein energy (DOPE) score obtained by MODELLER software is shown in Figure 2 from the finalized protein model. To determine whether the protein model can be used for docking studies, the accuracy of the model was verified using the Molprobity website. A web tool for structural validation called MolProbity offers a wide range of trustworthy model quality assessments for proteins and nucleic acids at both the global and local scales [15]. The Ramachandran plot acquired from the Molprobity was used to determine whether the protein model can be used for future research, including docking and other tests. In order to determine whether the protein itself can be used, the error must be identified, or the protein must be remodelled. The structural changes of the mutations and the wild-type do not impart significance. It is expected, as mutating a single

amino acid in *Pf*K13 does not give significant changes in the structure. However, the effects of these mutations are rather subtle [16]. Identifying the locations of the amino acids denoted by the black dots on the plot graph is one of the most important pieces of information from the Ramachandran plot. It is noteworthy to note that good Rama-Z scores are between -2.0 and 2.0 [17]. Based on the results presented in Table 1, it can be concluded that all four mutants and the wild-type have excellent Rama-Z scores.

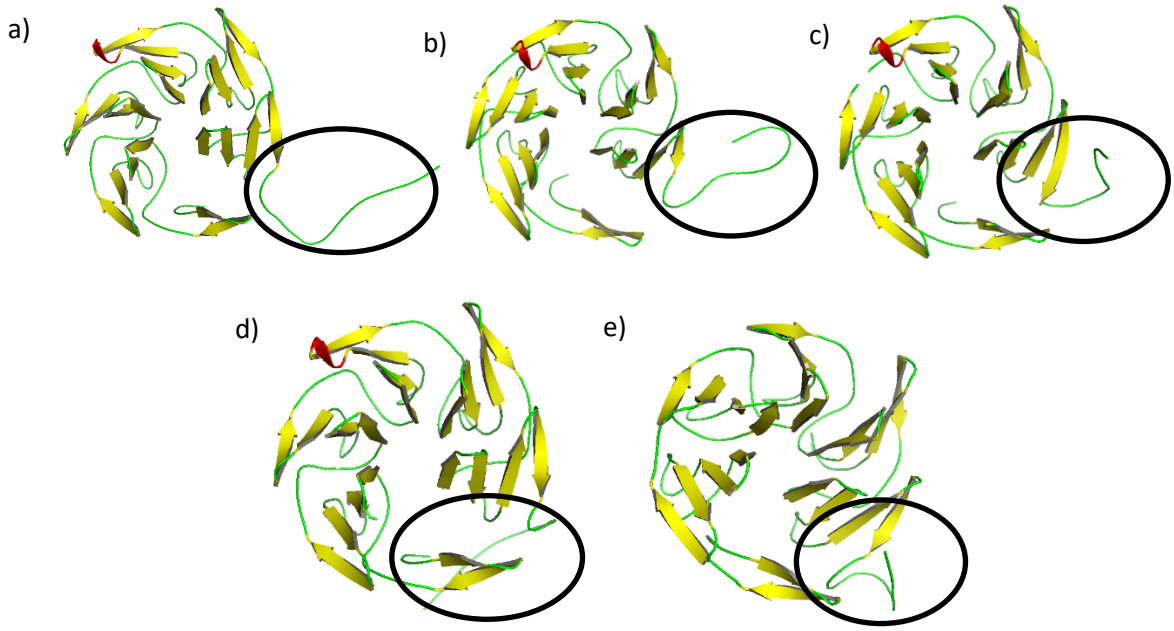

Fig. 2. a) The 3D protein model of the wild-type K13, b) The 3D protein model of V494I mutant, c) The 3D protein model of L598G mutant, d) The 3D protein model of S600C mutant, and e) The 3D protein model of N537I mutant. The alpha-helix is shown in red, β-sheet (yellow), and loop (green). The differences in these structures are circled at the CCC domain sites

Table 1
Rama distribution Z-score based on protein geometry result achieved from Molprobity website

No	*Protein mutant*	*Rama distribution Z-score*
1	Wild-type	-1.34 ± 0.45
2	V494I	-1.21 ± 0.42
3	L598G	-1.19 ± 0.41
4	S600C	-0.93 ± 0.43
5	N537I	-1.16 ± 0.43

For a more comprehensive examination of the Ramachandran plot graph, four factors were considered: the general case, isoleucine and valine plots, pre-proline plots, and glycine plots. In this study, there are no mutant cases that deviate from the norm, as depicted in Figure 3.

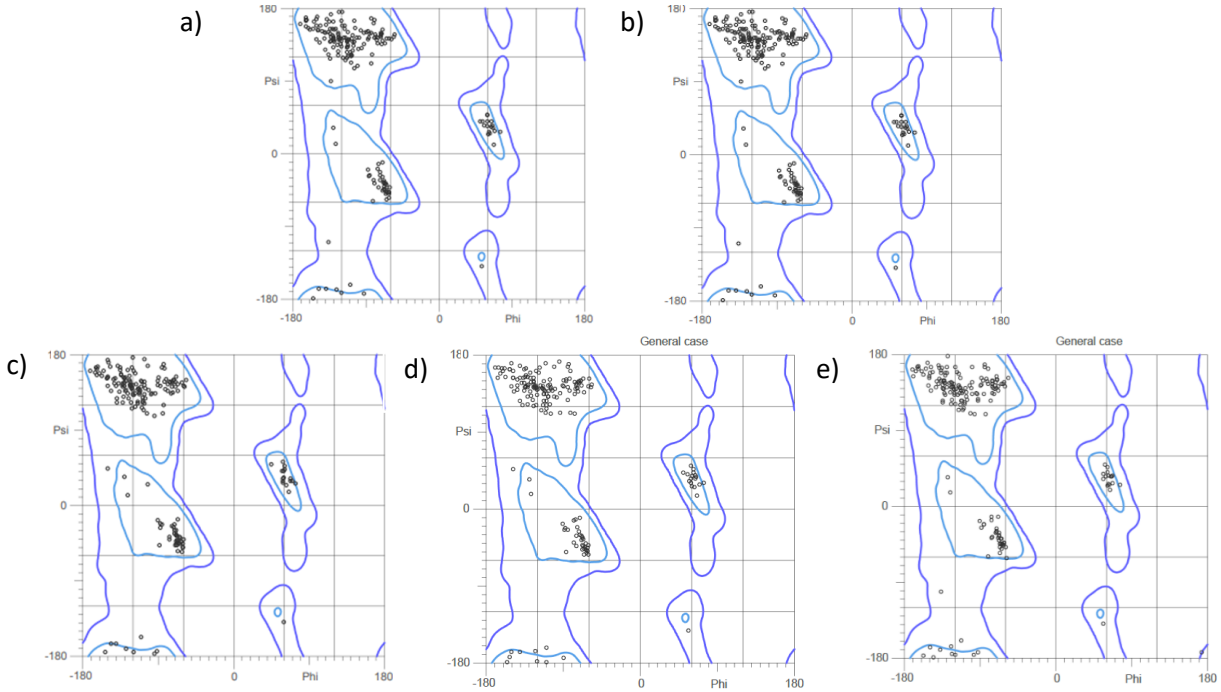

Fig. 3. General cases of Ramachandran plot of a) the K13 wild-type protein model, b) the K13 protein model of V494I mutant, c) the K13 protein model of L598G mutant, d) the K13 protein model of S600C mutant, and e) the K13 protein model of N537I mutant

The preferred or fully allowed region is denoted by light blue lines, whereas the permitted, or outer limit, region is denoted by a dark blue line, which could be used to label plot regions containing key secondary structures. The results indicate that the K13 protein wild-type model has 97.79% of available amino acids in the preferred region, whereas the V494I, L598G, S600C, and N537I protein mutants contain 97.01 %, 97.71%, 97.76%, and 97.05% of amino acids in the preferred region, respectively. As a result of these observations, it is possible to conclude that they are compatible with the Rama-Z scores, as they have high Rama Z-scores and a greater proportion of amino acids in the preferred region. This confirms the validity of the model's structure since high percentage indicates the model's high level of quality [1].

3.3 Docking Analysis

Molecular docking is a computer program used to determine how a compound binds to its target ligand. It is very useful in predicting the biological potency and binding affinity of small molecules [18]. In this study, a systematic computational approach was conducted to study the binding action of ART with *Pf*K13 protein, which aids in understanding the molecular basis of ART resistance towards V494I, L598G, S600C, and N537I mutations using Autodock Vina. Here, site-specific docking was carried out with the ART molecule acting as the ligand and the best quality of the generated protein models serving as the receptor. The CCC domain was used as the grid box's centre, with the grid points' x,y, and z coordinates set to 40,40,40 and their spacing set to 0.375.

The binding energy between the mutant protein and the ligand drug is shown in Table 2, where the binding energy between the mutant protein and the ligand drug revealed that the mutant structures showed lower binding energy compared to the wild-type K13 protein.

Table 2
Docking results between K13 proteins and ART obtained from Autodock Vina software

No.	*Protein mutant*	*Binding Energy (kcal/mol)*
1	Wild-type	-9.65
2	V494I	-6.79
3	L598G	-9.26
4	S600C	-6.17
5	N537I	-6.96

Table 2 shows that all the protein mutants indicate lower interaction stability between the protein and the drug. Binding energy per ligand atom to protein was used to determine ligand efficiency [12]. The better the ligand matches the receptor, the more stable the complex and the more negative the energy [8]. Non-covalent intermolecular interactions such as hydrogen bonding, electrostatic interactions, hydrophobic forces, and van der Waals forces between the two molecules affect binding affinity [19]. Hence, the docking interactions and bonding formations will be discussed further in the following section.

3.4 Binding Analysis between K13 Protein Mutants and ART

The balance of several energetic contributions, including hydrogen bonds, van der Waals forces, electrostatic forces, and the hydrophobic effect, determines how ligands and receptors attach to one another [20]. Figure 4 shows the location of the binding site for ART on the wild-type K13 protein. The hydrophobic interactions between the wild-type with ART is shown in Table 3, followed by hydrogen bond interactions in Table 4.

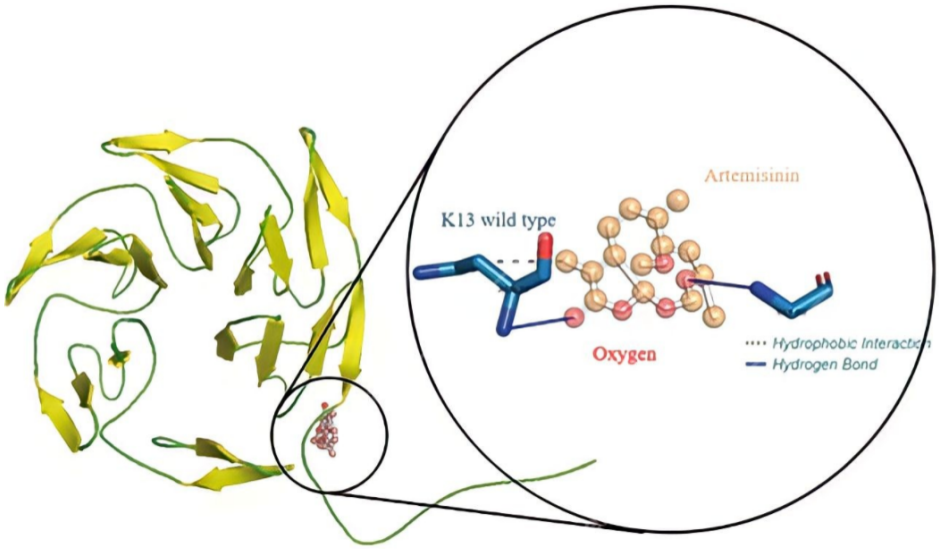

Fig. 4. Molecular interactions between ART and the wild-type K13 protein

LEU 255 residue is the most preferred hydrophobic interaction in the docking analysis of the wild-type protein, as shown in Table 3. Consequently, the CCC domain amino acids located at 212–341 should be the focal point of the findings in the V49VI, L598G, S600C and N537I protein mutants. The hydrogen bond that can form with ART is *via* CYS 243 residue as shown in Table 4. In order to change the binding affinity and drug efficacy, the ligands must be stabilised at the target site by hydrogen

bonding and hydrophobic interactions [21]. Hence, these interactions in the wild-type functioned as the control to compare the interactions that occur in all four mutations with ART.

Table 3
Hydrophobic interaction between the wild-type K13 protein and ART

Index	*Residue*	*AA*	*Distance(Å)*	*Ligand Atom*	*Protein atom*
1	255A	LEU	3.25	2689	2503

Table 4
Hydrogen bond interaction between the wild-type K13 protein and ART

	Residue	*AA*	*Distance H-A (Å)*	*Distance D-A (Å)*	*Donor Angle*	*Protein Donor*	*Side chain*	*Donor Atom*	*Acceptor Atom*
1	243A	CYS	2.79	3.14	100.34	✓	X	2375 [N3]	2675 [O2]

Meanwhile, Figures 5,6,7 and 8 show the location of the binding site for ART on the protein mutants. Subsequently, Tables 5,7,9 and 11 show the hydrophobic interactions between the protein mutants with ART. Meanwhile, the hydrogen bonds between the protein mutants with ART are shown in Tables 6,8,10 and 12.

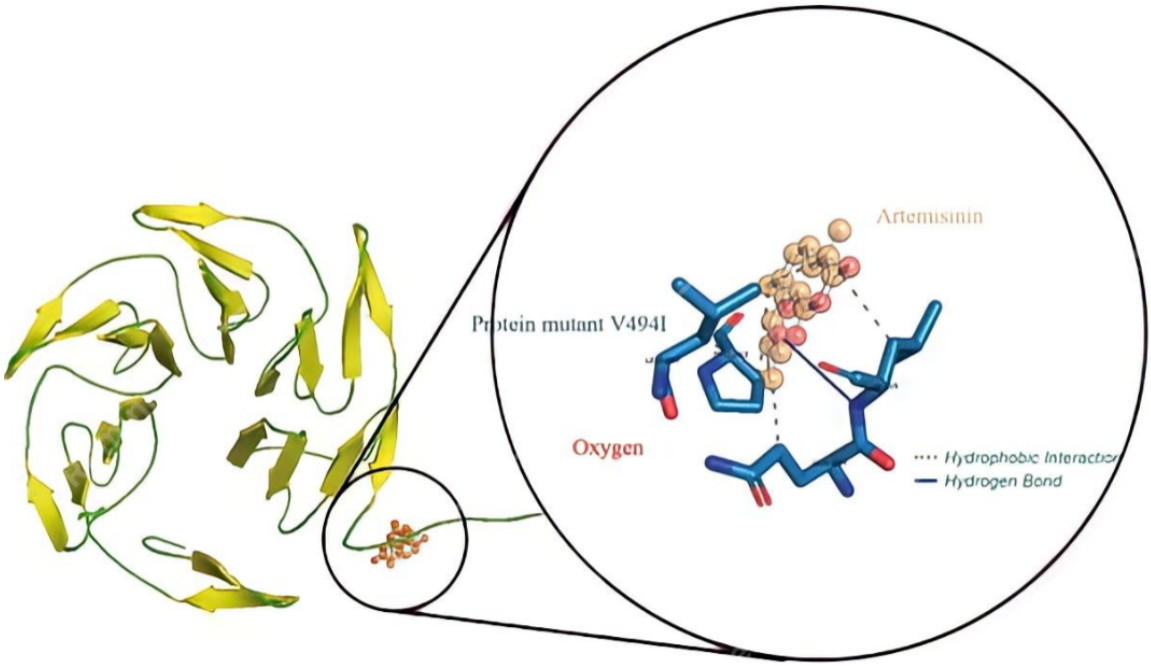

Fig. 5. Molecular interactions between ART and V494I protein mutant

Based on the results in Table 5, V494I protein mutant did not bind with the same residue as the wild-type, but it has at least five hydrophobic interactions, while it has only a hydrogen bond interaction with 255A residue, as shown in Table 6.

Table 5
Hydrophobic interactions between V494I and ART

Index	*Residue*	*AA*	*Distance(Å)*	*Ligand Atom*	*Protein atom*
1	254A	GLN	2.96	2687	2489
2	255A	LEU	3.84	2681	2500
3	260A	LEU	3.28	2687	2538
4	260A	LEU	3.56	2681	2540
5	262A	PRO	3.96	2684	2556

Table 6
Hydrogen bond between V494I and ART

Residue		*AA*	*Distance H-A (Å)*	*Distance D-A (Å)*	*Donor Angle*	*Protein Donor*	*Side chain*	*Donor Atom*	*Acceptor Atom*
1	255A	LEU	3.50	3.94	108.05	✓	X	2498 [N3]	2671 [O3]

Meanwhile, Figure 6 shows the location of the binding site for ART on L598G protein mutant and Table 7 shows the hydrophobic interactions between L598G protein with ART and the hydrogen bonds between L598G protein with ART are shown in Table 8.

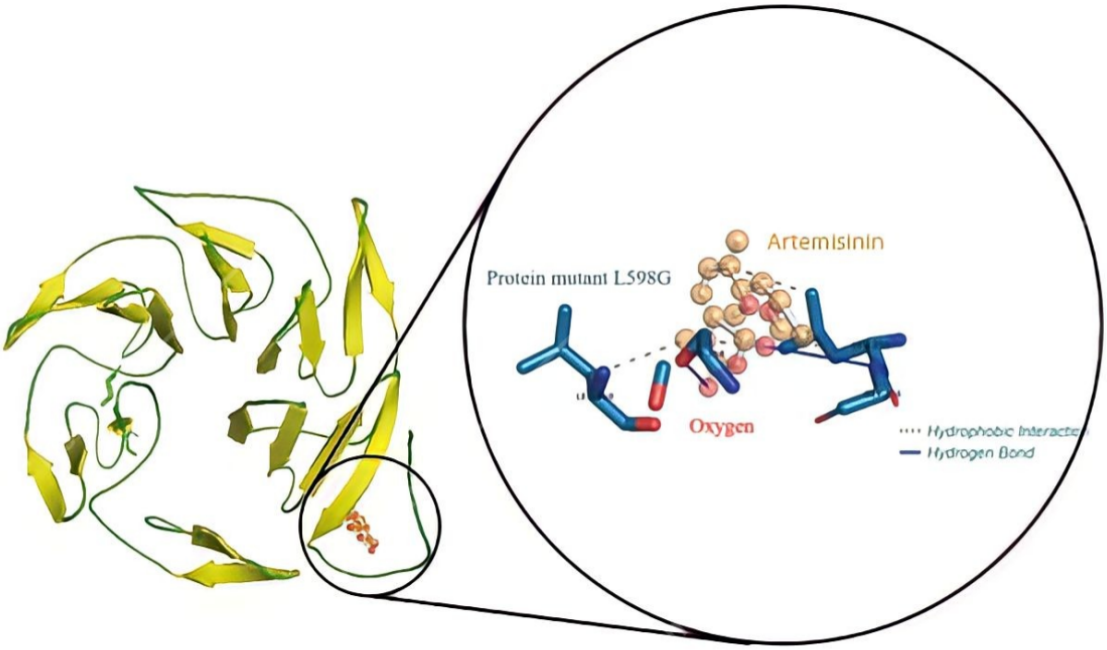

Fig. 6. Molecular interactions between ART and L598G protein mutant

Table 7
Hydrophobic interactions between L598G and ART

Index	*Residue*	*AA*	*Distance(Å)*	*Ligand Atom*	*Protein atom*
1	255A	LEU	3.54	2669	2482
2	255A	LEU	3.65	2658	2485
3	255A	LEU	3.48	2663	2484
4	260A	LEU	3.96	2668	2520

Table 8
Hydrogen bonds between L598G and ART

Residue		*AA*	*Distance H-A (Å)*	*Distance D-A (Å)*	*Donor Angle*	*Protein Donor*	*Side chain*	*Donor Atom*	*Acceptor Atom*
1	256A	GLY	3.51	4.06	115.64	✓	X	2489 [N3]	2651 [O2]
2	258A	SER	3.04	3.68	125.44	✓	✓	2504 [O3]	2654 [O2]

The L598G protein mutant, unlike the V494I protein mutant, has the same hydrophobic interaction between ART ligand with the wild-type protein, but it has three interactions with residue LEU 255 that differ in distance, ligand atom, and protein atom, as shown in Table 8.

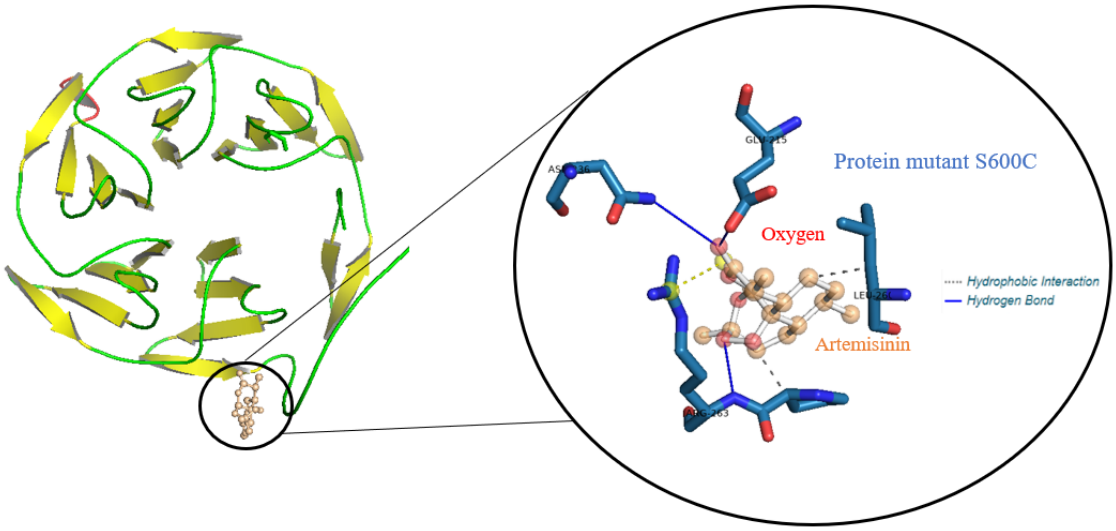

Fig. 7. Molecular interactions between ART and S600C protein mutant

Meanwhile, in Figure 7, the location of the binding site for the ART on the S600C protein was observed. Table 9 shows the hydrophobic interactions between S600C protein with ART, while the hydrogen bonds between S600C protein with ART are shown in Table 10.

Table 9
Hydrophobic interactions between S600C and ART

Index	*Residue*	*AA*	*Distance(Å)*	*Ligand Atom*	*Protein atom*
1	260A	LEU	3.38	2683	2539
2	262A	PRO	3.47	2680	2557

Table 10
Hydrogen bonds between S600C and ART

Residue		*AA*	*Distance H-A (Å)*	*Distance D-A (Å)*	*Donor Angle*	*Protein Donor*	*Side chain*	*Donor Atom*	*Acceptor Atom*
1	215A	GLU	2.20	2.87	127.68	✓	✓	2127 [O3]	2676 [O2]
2	236A	ASN	2.89	3.63	146.07	✓	✓	2315 [O3]	2676 [O2]
3	263A	ARG	2.20	3.05	170.96	✓	X	2561 [Nam]	2688 [O3]

Based on the results from Table 9, the S600C protein mutant did not bind with the same residue as the wild-type, but it has at least two hydrophobic interactions, and it has three hydrogen bonds, as shown in Table 10.

Subsequently, Figure 8 indicates the location of the binding site for the ART on the N537I protein mutant. Table 11 tabulates the hydrophobic interactions between N537I protein with ART and the hydrogen bonds between N537I protein with ART are shown in Table 12.

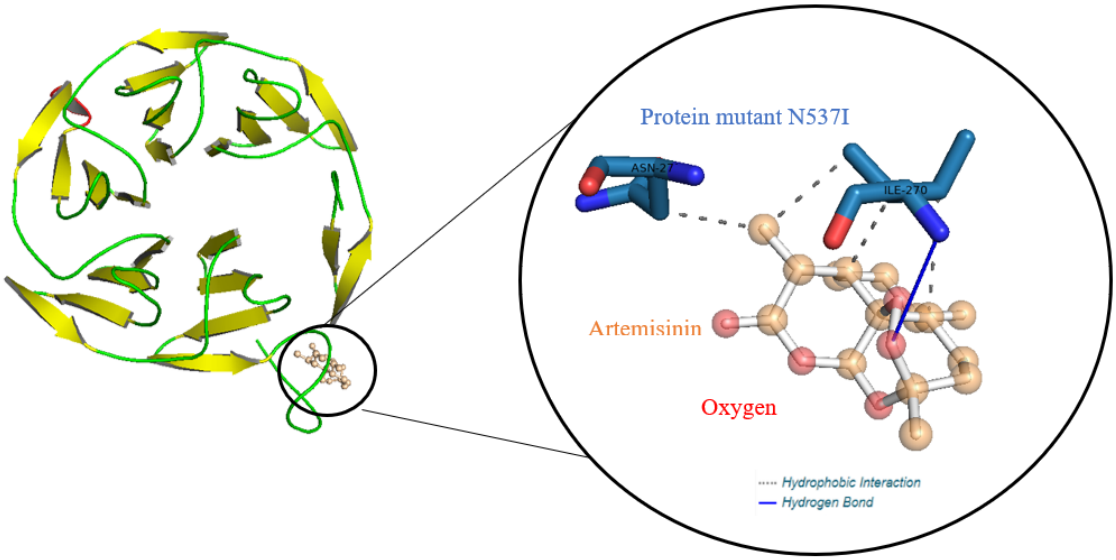

Fig. 8. Molecular interactions between ART and N537I protein mutant

Table 11
Hydrophobic interactions between N537I and ART

Index	*Residue*	*AA*	*Distance(Å)*	*Ligand Atom*	*Protein atom*
1	270A	ILE	3.32	2679	2641
2	270A	ILE	3.03	2686	2639
3	270A	ILE	3.68	2691	2640
4	272A	ASN	3.43	2679	2654

Table 12
Hydrogen bond between N537I and ART

	Residue	*AA*	*Distance H-A (Å)*	*Distance D-A (Å)*	*Donor Angle*	*Protein Donor*	*Side chain*	*Donor Atom*	*Acceptor Atom*
1	270A	ILE	2.40	3.26	175.85	✓	X	2637 [Nam]	2692 [O3]

The results from Table 11 show the N537I protein mutant did not bind with the same residue as the wild-type, but it has at least four hydrophobic interactions and only one hydrogen bond, as shown in Table 12.

The hydrophobic factor affects the energetic preference of non-polar molecular surfaces to interact with other non-polar molecular surfaces, displacing water molecules from the interacting surfaces. The hydrophobic effect is contributed to by both enthalpic and entropic effects. Hydrophobic interactions are alluring, short-range interactions that significantly contribute to ligand-receptor binding affinities. They contribute to specificity in the same manner as hydrogen bonding interactions, but in a manner that is less constrained geometrically [22].

It was reported that hydrophobic interactions predominate and make a significant contribution, whereas hydrogen bonding and polar interactions aid in the correct orientation of a compound (or functional group) for maximum interaction [23]. Meanwhile, the energetics of the protein-ligand hydrogen bonds cannot be determined from a single snapshot or the total number of bonds since other factors, such as the makeup of the binding site residues, may have an impact on this scaling relationship [24]. Additionally, mixed strong-weak hydrogen bond pairings explained why indiscriminately increasing receptor-ligand hydrogen bonds are weakly connected with experimental binding affinity and reduce ligand-binding affinity due to bulk water interference [25].

Even though the function of the K13 protein is still unknown, but there are studies on the mechanism of this protein which revealed that this protein is potentially involved in the unfolded protein response (UPR) pathway, protein folding, protein binding, translation and oxidative stress responses [26]. Besides that, one study indicates that an up-regulated UPR may be a major mediator of ART resistance in *P. falciparum* and is caused by single K13 propeller mutation [27]. However, the mechanism might be hard to deduce in the *in silico* study since the mutation is a point mutation, hence structure change is not significantly distinctive compared to the wild-type. Hence, the predictions obtained from this study have to be further confirmed in experimental analysis such as Isothermal Titration Calorimetry (ITC) to prove the binding energy.

4. Conclusions

Although K13 is believed to bind substrate proteins, its functional or interaction sites and the structural changes associated with mutations that lead to ART resistance are still unclear. Aligning the protein sequences of the mutant and wild-type organisms revealed that they are 91% identical, with minor differences in certain regions. The Modeller software generated a 3D model of the protein structure that was suitable for docking based on the proportion of the region with the highest preference. Based on the docking tests, we can conclude that all the V494I, L598G, N537I and S600C protein mutants formed complexes with less stability compared to the wild-type K13 protein, due to a decrease in the negative value of binding energy. As a result, the mutations might have reduced the efficacy of ART. However, the number of hydrophobic and hydrogen bonds formed between these four mutants and ART are higher compared to the wild-type, indicating stronger interactions that require future experimental determination to assess the effectiveness of ART against the K13 protein mutants.

Acknowledgment

The authors would like to thank the Director General of Health Malaysia for his permission to publish this article. The study was supported by the Ministry of Health Malaysia Research Grant (NMRR-21-1175-60416). The funders had no role in the study design, data collection analysis, or preparation of the manuscript. We also thank the Parasitology Unit, Infectious Disease Research Centre, Institute for Medical Research, Institute of National Health, Setia Alam and Department of Chemical Engineering & Sustainability (CHES), Kulliyyah of Engineering, International Islamic University Malaysia for their assistance in performing these studies. This study has been approved by the MREC number 21-1175-60416.

References

[1] Banerjee, Amit Kumar, Neelima Arora, and U. S. N. Murty. "Analyzing a potential drug target N-Myristoyltransferase of Plasmodium falciparum through in silico approaches." *Journal of Global Infectious Diseases* 4, no. 1 (2012): 43. https://doi.org/10.1016/S1878-6480(12)70533-5

[2] Meshnick, Steven R. "Artemisinin: mechanisms of action, resistance and toxicity." *International journal for parasitology* 32, no. 13 (2002): 1655-1660. https://doi.org/10.1016/S0020-7519(02)00194-7

[3] Tilley, Leann, Judith Straimer, Nina F. Gnädig, Stuart A. Ralph, and David A. Fidock. "Artemisinin action and resistance in Plasmodium falciparum." *Trends in parasitology* 32, no. 9 (2016): 682-696. https://doi.org/10.1016/j.pt.2016.05.010

[4] Mok, Sachel, Barbara H. Stokes, Nina F. Gnädig, Leila S. Ross, Tomas Yeo, Chanaki Amaratunga, Erik Allman et al. "Artemisinin-resistant K13 mutations rewire Plasmodium falciparum's intra-erythrocytic metabolic program to enhance survival." *Nature communications* 12, no. 1 (2021): 1-15. https://doi.org/10.1038/s41467-020-20805-w

[5] Coppée, Romain, Daniel C. Jeffares, Maria A. Miteva, Audrey Sabbagh, and Jérôme Clain. "Comparative structural and evolutionary analyses predict functional sites in the artemisinin resistance malaria protein K13." *Scientific reports* 9, no. 1 (2019): 1-17. https://doi.org/10.1038/s41598-019-47034-6

[6] Blasco, Benjamin, Didier Leroy, and David A. Fidock. "Antimalarial drug resistance: linking Plasmodium falciparum parasite biology to the clinic." *Nature medicine* 23, no. 8 (2017): 917-928. https://doi.org/10.1038/nm.4381

[7] Onchieku, Noah Machuki, Sonam Kumari, Rajan Pandey, Vaibhav Sharma, Mohit Kumar, Arunaditya Deshmukh, Inderjeet Kaur et al. "Artemisinin Binds and Inhibits the Activity of Plasmodium falciparum Ddi1, a Retroviral Aspartyl Protease." *Pathogens* 10, no. 11 (2021): 1465. https://doi.org/10.3390/pathogens10111465

[8] Samah, Farhana Abu, Siti Zalita Talib, Nur Ainun Mokhtar, and Nurulbahiyah Ahmad Khairudin. "Molecular Docking Studies Of Potential Drugs For Covid19 Targetting On The Coronavirus Hemagglutinin Esterase." *Journal of Research in Nanoscience and Nanotechnology* 4, no. 1 (2021): 13-18.

[9] Di Tommaso, Paolo, Sebastien Moretti, Ioannis Xenarios, Miquel Orobitg, Alberto Montanyola, Jia-Ming Chang, Jean-Francois Taly, and Cedric Notredame. "T-Coffee: a web server for the multiple sequence alignment of protein and RNA sequences using structural information and homology extension." *Nucleic acids research* 39, no. suppl_2 (2011): W13-W17. https://doi.org/10.1093/nar/gkr245

[10] Chang, Jia-Ming, Paolo Di Tommaso, and Cedric Notredame. "TCS: a new multiple sequence alignment reliability measure to estimate alignment accuracy and improve phylogenetic tree reconstruction." *Molecular biology and evolution* 31, no. 6 (2014): 1625-1637. https://doi.org/10.1093/molbev/msu117

[11] Mok, Sachel, Barbara H. Stokes, Nina F. Gnädig, Leila S. Ross, Tomas Yeo, Chanaki Amaratunga, Erik Allman et al. "Artemisinin-resistant K13 mutations rewire Plasmodium falciparum's intra-erythrocytic metabolic program to enhance survival." *Nature communications* 12, no. 1 (2021): 1-15. https://doi.org/10.1038/s41467-020-20805-w

[12] Yusuf, NoorAzian Md, Afiqah Saleh Huddin, Jose Miguel Rubio, Mohd Ridzuan Mohd Abd Razak, Nurul Shuhada Mohd Ali, Renuka Devi, MacCallyster Anak Isa et al. "PREVALENCE OF PLASMODIUM FALCIPARUM KELCH13 POLYMORPHISMS IN MALAYSIA (2008-2017)." *Southeast Asian Journal of Tropical Medicine and Public Health* 51, no. 1 (2020): 8-17.

[13] di Luccio, Eric, and Patrice Koehl. "A quality metric for homology modeling: the H-factor." *BMC bioinformatics* 12, no. 1 (2011): 1-19. https://doi.org/10.1186/1471-2105-12-48

[14] Shen, Min-yi, and Andrej Sali. "Statistical potential for assessment and prediction of protein structures." *Protein science* 15, no. 11 (2006): 2507-2524. https://doi.org/10.1110/ps.062416606

[15] Chen, Vincent B., W. Bryan Arendall, Jeffrey J. Headd, Daniel A. Keedy, Robert M. Immormino, Gary J. Kapral, Laura W. Murray, Jane S. Richardson, and David C. Richardson. "MolProbity: all-atom structure validation for macromolecular crystallography." *Acta Crystallographica Section D: Biological Crystallography* 66, no. 1 (2010): 12-21.

[16] Patel, Chandan, and Dipankar Roy. "A computational study of molecular mechanism of chloroquine resistance by chloroquine resistance transporter protein of plasmodium falciparum via molecular modeling and molecular simulations." *Physchem* 1, no. 3 (2021): 232-242. https://doi.org/10.3390/physchem1030017

[17] Sobolev, Oleg V., Pavel V. Afonine, Nigel W. Moriarty, Maarten L. Hekkelman, Robbie P. Joosten, Anastassis Perrakis, and Paul D. Adams. "A global Ramachandran score identifies protein structures with unlikely stereochemistry." *Structure* 28, no. 11 (2020): 1249-1258. https://doi.org/10.1016/j.str.2020.08.005

[18] Zakaria, Nur Hanis, LAMKOK WAI, and Nurul Izzaty Hassan. "Molecular docking study of the interactions between Plasmodium falciparum lactate dehydrogenase and 4-aminoquinoline hybrids." *Sains Malaysiana* 49, no. 8 (2020): 1905-1913. https://doi.org/10.17576/jsm-2020-4908-12

[19] Pantsar, Tatu, and Antti Poso. 2018. "Molecules Opinion Binding Affinity via Docking: Fact and Fiction." https://doi.org/10.3390/molecules23081899. https://doi.org/10.3390/molecules23081899

[20] Motiejunas, D., and R. C. Wade. "Structural, energetic, and dynamic aspects of ligand–receptor interactions." (2007): 193-213. https://doi.org/10.1016/B0-08-045044-X/00250-9

[21] Patil, Rohan, Suranjana Das, Ashley Stanley, Lumbani Yadav, Akulapalli Sudhakar, and Ashok K. Varma. "Optimized hydrophobic interactions and hydrogen bonding at the target-ligand interface leads the pathways of drug-designing." *PloS one* 5, no. 8 (2010): e12029. https://doi.org/10.1371/journal.pone.0012029

[22] Motiejunas, D., and R. C. Wade. "Structural, energetic, and dynamic aspects of ligand–receptor interactions." (2007): 193-213. https://doi.org/10.1016/B0-08-045044-X/00250-9

[23] Sahu, V. K., A. K. R. Khan, R. K. Singh, and P. P. Singh. "Hydrophobic, polar and hydrogen bonding based drug-receptor interaction of tetrahydroimidazobenzodiazepinones." *Am. J. Immunol* 4, no. 3 (2008): 33. https://doi.org/10.3844/ajisp.2008.33.42

[24] Nnyigide, Osita Sunday, Sun-Gu Lee, and Kyu Hyun. "In silico characterization of the binding modes of surfactants with bovine serum albumin." *Scientific reports* 9, no. 1 (2019): 1-16. https://doi.org/10.1038/s41598-019-47135-2

[25] Chen, Deliang, Numan Oezguen, Petri Urvil, Colin Ferguson, Sara M. Dann, and Tor C. Savidge. "Regulation of protein-ligand binding affinity by hydrogen bond pairing." *Science advances* 2, no. 3 (2016): e1501240. https://doi.org/10.1126/sciadv.1501240

[26] Bhattacharjee, Souvik, Isabelle Coppens, Alassane Mbengue, Niraja Suresh, Mehdi Ghorbal, Zdenek Slouka, Innocent Safeukui et al. "Remodeling of the malaria parasite and host human red cell by vesicle amplification that induces artemisinin resistance." *Blood, The Journal of the American Society of Hematology* 131, no. 11 (2018): 1234-1247. https://doi.org/10.1182/blood-2017-11-814665

[27] Siddiqui, Faiza Amber, Rachasak Boonhok, Mynthia Cabrera, Huguette Gaelle Ngassa Mbenda, Meilian Wang, Hui Min, Xiaoying Liang et al. "Role of Plasmodium falciparum Kelch 13 protein mutations in P. falciparum populations from northeastern Myanmar in mediating artemisinin resistance." *MBio* 11, no. 1 (2020): e01134-19. https://doi.org/10.1128/mBio.01134-19